



Late-time H/He-poor Circumstellar Interaction in the Type Ic Supernova SN 2021ocs: An Exposed Oxygen–Magnesium Layer and Extreme Stripping of the Progenitor*

H. Kuncarayakti^{1,2}, K. Maeda³, L. Dessart⁴, T. Nagao¹, M. Fulton⁵, C. P. Gutiérrez^{1,2}, M. E. Huber⁶, D. R. Young⁵, R. Kotak¹, S. Mattila^{1,7}, J. P. Anderson^{8,9}, L. Ferrari^{10,11}, G. Folatelli^{10,11,12}, H. Gao⁶, E. Magnier⁶, K. W. Smith⁵, and S. Srivastav⁵

¹ Tuorla Observatory, Department of Physics and Astronomy, FI-20014 University of Turku, Finland

² Finnish Centre for Astronomy with ESO (FINCA), FI-20014 University of Turku, Finland

³ Department of Astronomy, Graduate School of Science, Kyoto University, Sakyo-ku, Kyoto 606-8502, Japan

⁴ Institut d’Astrophysique de Paris, CNRS-Sorbonne Université, 98 bis boulevard Arago, F-75014 Paris, France

⁵ Astrophysics Research Centre, School of Mathematics and Physics, Queen’s University Belfast, Belfast, BT7 1NN, UK

⁶ Institute for Astronomy, University of Hawaii, 2680 Woodlawn Drive, Honolulu, HI 96822, USA

⁷ School of Sciences, European University Cyprus, Diogenes Street, Engomi, 1516 Nicosia, Cyprus

⁸ European Southern Observatory, Alonso de Córdova 3107, Casilla 19, Santiago, Chile

⁹ Millennium Institute of Astrophysics MAS, Nuncio Monsenor Sotero Sanz 100, Off. 104, Providencia, Santiago, Chile

¹⁰ Facultad de Ciencias Astronómicas y Geofísicas, Universidad Nacional de La Plata, Paseo del Bosque S/N, B1900FWA La Plata, Argentina

¹¹ Instituto de Astrofísica de La Plata (IALP), CONICET, Argentina

¹² Kavli Institute for the Physics and Mathematics of the Universe (WPI), The University of Tokyo, 5-1-5 Kashiwanoha, Kashiwa, Chiba 277-8583, Japan

Received 2022 October 3; revised 2022 November 19; accepted 2022 November 27; published 2022 December 19

Abstract

Supernova (SN) 2021ocs was discovered in the galaxy NGC 7828 ($z = 0.01911$) within the interacting system Arp 144 and subsequently classified as a normal Type Ic SN around peak brightness. Very Large Telescope/FORS2 observations in the nebular phase at 148 days reveal that the spectrum is dominated by oxygen and magnesium emission lines of different transitions and ionization states: O I, [O I], [O II], [O III], Mg I, and Mg II. Such a spectrum has no counterpart in the literature, though it bears a few features similar to those of some interacting Type Ibn and Icn SNe. Additionally, SN 2021ocs showed a blue color, $(g - r) \lesssim -0.5$ mag, after the peak and up to late phases, atypical for a Type Ic SN. Together with the nebular spectrum, this suggests that SN 2021ocs underwent late-time interaction with an H/He-poor circumstellar medium (CSM) resulting from the pre-SN progenitor mass loss during its final ~ 1000 days. The strong O and Mg lines and the absence of strong C and He lines suggest that the progenitor star’s O–Mg layer is exposed, which places SN 2021ocs as the most extreme case of a massive progenitor star’s envelope stripping in interacting SNe, followed by Type Icn (stripped C–O layer) and Ibn (stripped He-rich layer) SNe. This is the first time such a case is reported in the literature. The SN 2021ocs emphasizes the importance of late-time spectroscopy of SNe, even for those classified as normal events, to reveal the inner ejecta and progenitor star’s CSM and mass loss.

Unified Astronomy Thesaurus concepts: Supernovae (1668); Core-collapse supernovae (304); Ejecta (453); Circumstellar matter (241); Massive stars (732); Late stellar evolution (911); Wolf-Rayet stars (1806)

Supporting material: data behind figures

1. Introduction

Stripped-envelope supernovae (SESNe) include a broad variety of events, all of which show little or no hydrogen in the spectrum. Type Ic SNe are deficient in H and He; hence, the progenitors are traditionally thought to be Wolf-Rayet (W-R) stars (e.g., Woosley et al. 1995). The progenitor stars of SESNe require significant mass loss in order to remove the outer H envelope. Stellar winds, binary interaction, and eruptions are among the prominent mechanisms (see, e.g., Smith 2014, for a review). A highly massive single star ($M_{\text{ZAMS}} \gtrsim 25 M_{\odot}$) is required to form a W-R star through wind stripping. This casts doubt if there is sufficient number of W-R stars to explain the observed rate of SESNe, which implies that a significant

number of SESNe must have come from lower-mass stars in close binary systems (e.g., Yoon et al. 2010; Smith et al. 2011).

The SN progenitor mass loss may result in a circumstellar medium (CSM), which may interact with the SN ejecta after the explosion. The SNe interacting with H-free CSM are rare; nevertheless, modern surveys have discovered a sample of them, which are now classified into Types Ibn (He-rich CSM) and Icn (H/He-poor CSM). Some of these objects are thought to be explosions of genuine massive W-R stars (Pastorello et al. 2007; Smith 2017; Gal-Yam et al. 2022) or less massive stars (Sanders et al. 2013; Davis et al. 2022; Dessart et al. 2022; Pellegrino et al. 2022) within a dense CSM.

The SN 2021ocs was discovered by the Asteroid Terrestrial-impact Last Alert System (ATLAS) survey (Tonry et al. 2018; Smith et al. 2020) on 2021 May 30 (UTC time used throughout) as ATLAS21ptp, in the host galaxy NGC 7828 ($z = 0.01911$, Tully–Fisher distance modulus $\mu = 34.71$ mag; Theureau et al. 2007, through NED¹³). The host galaxy is interacting with a smaller galaxy, NGC 7829, forming the ring

* Based on observations collected at the European Organisation for Astronomical Research in the Southern Hemisphere under ESO program 108.2282.001.



Original content from this work may be used under the terms of the [Creative Commons Attribution 4.0 licence](https://creativecommons.org/licenses/by/4.0/). Any further distribution of this work must maintain attribution to the author(s) and the title of the work, journal citation and DOI.

¹³ The NASA/IPAC Extragalactic Database (NED), <http://ned.ipac.caltech.edu/>.

galaxy system Arp 144. No meaningful prediscovery upper limit exists, as the object was emerging from solar conjunction at the time of discovery. The transient was subsequently reported to the Transient Name Server (TNS¹⁴) by the Zwicky Transient Facility (ZTF; Bellm et al. 2019) and Pan-STARRS1 (Chambers et al. 2016) surveys as ZTF21abhrpia and PS21h1k, respectively. Spectral classification reported to the TNS suggests that SN 2021ocs is a Type Ic SN around 1–2 weeks after maximum light (Huber 2021). Here we report additional spectral observations of SN 2021ocs obtained at late time (148 days after light-curve peak).¹⁵

2. Observations and Data Reduction

The classification spectrum of SN 2021ocs was obtained on 2021 June 13 using the SNIFS spectrograph (Lantz et al. 2004) at the 2.2 m University of Hawaii telescope on Maunakea as part of the Spectroscopic Classification of Astronomical Transients survey (Tucker et al. 2022). Late-time spectroscopy of SN 2021ocs was conducted on the night of 2021 October 26 as part of the FORS+ Survey of Supernovae in Late Times program (FOSSIL; H. Kuncarayakti et al. 2022, in preparation) using the FORS2 instrument (Appenzeller et al. 1998) attached to the ESO Very Large Telescope at Cerro Paranal Observatory, Chile. FOSSIL targets all observable core-collapse SNe (CCSNe) brighter than ~ 18.5 mag in the photospheric phase, which are expected to be ~ 21 – 22 mag or brighter when observed in the nebular phase, with the goal of obtaining nebular spectra for a large sample of objects in a magnitude-limited, unbiased way.

We used FORS2 with grism 300V and the $1''.6$ slit, achieving a wide wavelength coverage of 3500–9500 Å and a spectral resolution of $R \sim 400$ measured from the narrow sky emission lines. The sky conditions were photometric with seeing around $0''.5$ during the length of the integration. The spectroscopic observations were obtained with 2×1300 s exposures accompanied by 20 s g -band imaging under $0''.75$ seeing conditions. Spectrophotometric standard stars were observed using the same grism setting. The data were reduced using the ESOReflex (Freudling et al. 2013) pipeline following standard procedures. The excellent seeing conditions allowed reasonable background subtraction during the spectrum extraction, evidenced by the absence of narrow host galaxy emission lines.

The g -band photometry of FORS2 was measured with our own point-spread function photometry code. Synthetic photometry was performed on the nebular spectrum to derive the g and r synthetic magnitudes; the obtained $(g - r)$ color was then applied to the g -band photometry from imaging to produce an r -band magnitude to be used in the light curve. In addition to the FORS2 gr imaging, photometry was obtained from a number of sources. Public ATLAS forced photometry in the o and c bands was obtained from the ATLAS Forced Photometry server,¹⁶ and ZTF g - and r -band photometry was obtained through the ZTF forced photometry service¹⁷ (Masci et al. 2019). Forced photometry data from the Pan-STARRS1 survey are used, yielding i - and w -band photometry.

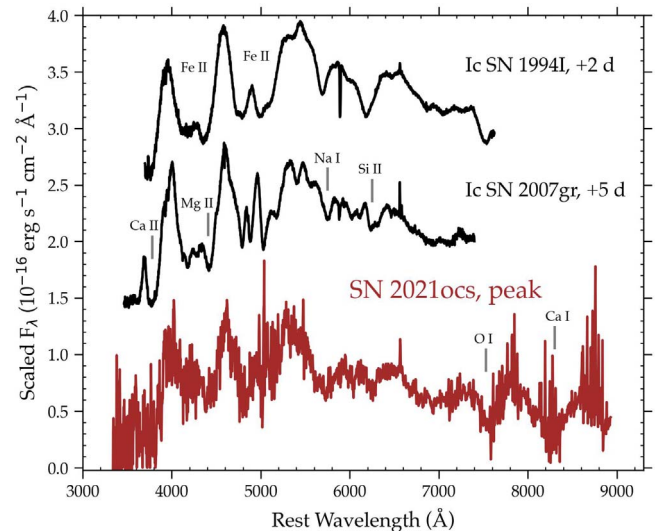


Figure 1. Classification spectrum of SN 2021ocs obtained shortly after the light-curve peak compared to those of well-observed Type Ic SNe at similar epochs. The spectra and phases (defined as time relative to the light-curve peak throughout the paper) of the comparison objects were taken from the WISEREP repository (Yaron & Gal-Yam 2012), originally from Modjaz et al. (2014). Prominent absorption features typical of Type Ic SNe are indicated.

3. Results and Discussion

3.1. Early Spectrum and Light Curve

The classification of SN 2021ocs as a Type Ic SN around the light-curve peak (Huber 2021) was obtained using the SNID tool (Blondin & Tonry 2007). Figure 1 shows a comparison between SN 2021ocs and the well-studied Type Ic SNe SN 1994I and SN 2007gr as two of the best matches obtained by SNID. The SN 2021ocs appears similar to normal Type Ic SNe around the light-curve peak. The lack of a narrow Na I D $\lambda\lambda 5889, 5896$ absorption line in the spectrum (see SN 1994I, where the narrow absorption line is strong, and weaker in SN 2007gr) suggests that the amount of intervening extinction is minimal. Henceforth, we assume no host galaxy extinction for SN 2021ocs. The reported foreground extinction for NGC 7828 is similarly negligible, as it is at the level of the photometric uncertainty, $A_V = 0.086$ mag (Schlafly & Finkbeiner 2011, via NED).

While the light curves of SN 2021ocs are not very well sampled, the earliest data points from ATLAS suggest that it was rising in brightness (Figure 2(a)), and the subsequent epochs indicate that it declined steadily, as is typical for most SESN light curves, though with slight fluctuations. Comparing to the templates of early-time light curves of SNe Ib/c (Taddia et al. 2015), it appears that the peak of the light curve occurred around a week after the brightest point in the photometry, which implies that the classification spectrum was taken within 1–2 weeks from the peak brightness, consistent with the phase determined from spectral matching. The comparison between the light curves and the templates suggests that SN 2021ocs peaked around $M \sim -16.7$ mag, which is fainter than most SESNe but still within the range of the previously observed objects (Taddia et al. 2015; Zheng et al. 2022; see also, e.g., Perley et al. 2020, Figure 7). Alternatively, the peak could have occurred during the solar conjunction before the first detections, which would imply that the light curve could be broader and more luminous. However, in this case, the classification spectrum would suggest a considerably older phase. This

¹⁴ <https://www.wis-tns.org/object/2021ocs>

¹⁵ The spectrum and light curves are available as the Data behind the Figure.

¹⁶ <https://fallingstar-data.com/forcedphot/>

¹⁷ <https://ztfweb.ipac.caltech.edu/cgi-bin/requestForcedPhotometry.cgi>

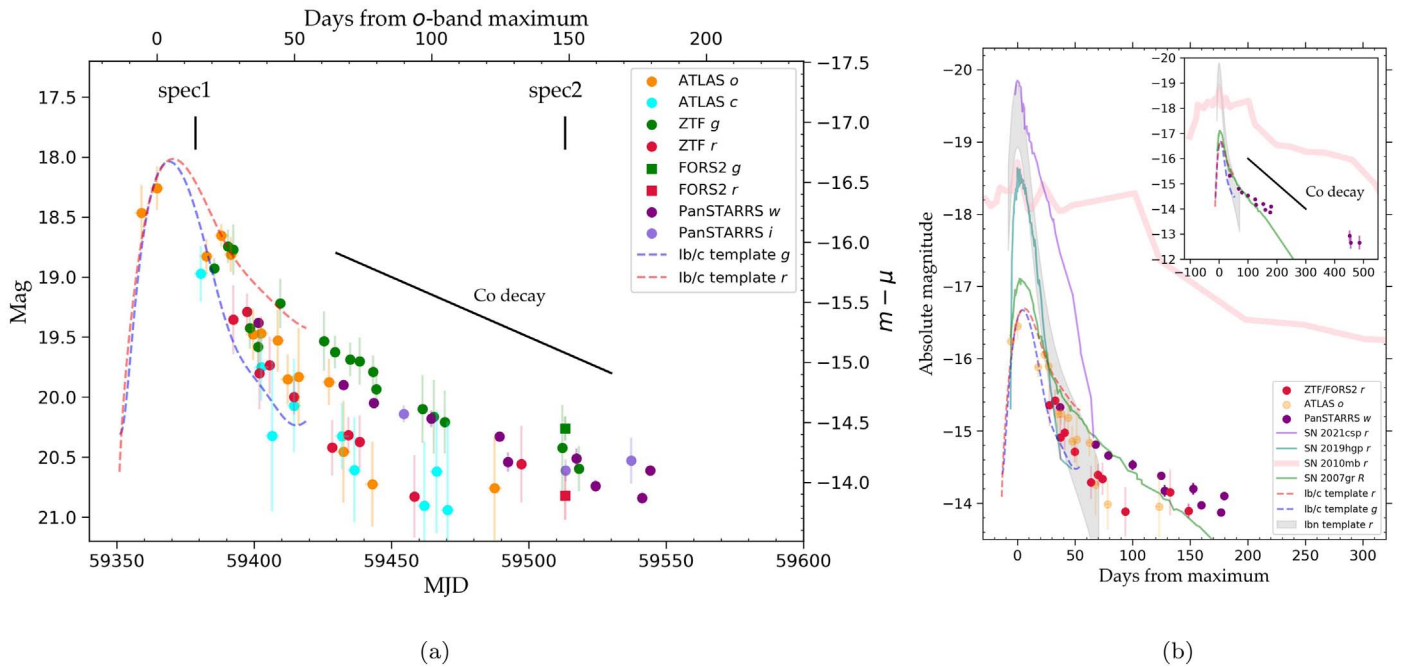


Figure 2. (a) Light curves of SN 2021ocs in ATLAS o (orange symbols) and c (cyan) with 5 day binning, ZTF 3 day binned 5σ detections and FORS2 in g (green) and r (red), and Pan-STARRS w (dark purple) and i (light purple) bands. The template SN Ib/c light curves from Taddia et al. (2015) are plotted with dashed lines (blue for g and red for r). The epochs of the first (classification) and second (nebular) spectra are indicated, along with the radioactive ^{56}Co decay rate assuming complete γ -ray trapping ($0.01 \text{ mag day}^{-1}$). The ATLAS c bandpass corresponds roughly to the $g + r$ bands, while o covers $r + i$. The Pan-STARRS w band is a white-light bandpass covering the gri bands. (b) Absolute-magnitude light-curve comparison against well-observed Type Icn SNe 2010mb (Ben-Ami et al. 2014), 2019hgp (Gal-Yam et al. 2022), and 2021csp (Perley et al. 2022). The SN 2010mb is a peculiar case of Icn-related objects with its broad light curve. A light-curve template of SNe Icn (Hosseinzadeh et al. 2017) is also plotted alongside the Ib/c templates and the R -band light curve of SN 2007gr ($\mu = 29.84 \text{ mag}$; Hunter et al. 2009). The inset shows a wider phase range covering Pan-STARRS late detections.

(The data used to create this figure are available.)

alternative scenario cannot be ruled out but requires strong additional assumptions on the early spectral evolution in order to be consistent with the classification spectrum.

In Figure 2(b), the light curves of SN 2021ocs are compared with those of SN 2007gr¹⁸ and H-poor interacting SNe (see Section 3.3). Assuming typical early SN Ic evolution, SN 2021ocs shows a gradual decline after the light-curve peak. In general, SN 2021ocs shows a slower decline compared to the Ib/Icn population, although there exist individual objects that exhibit significantly broader light curves (e.g., Ben-Ami et al. 2014; Kool et al. 2021).

While the light-curve peak brightness and width are unlikely to diverge significantly compared to the bulk of SESNe, SN 2021ocs appears to be peculiarly blue from the first detections in the g and r bands up until late phases.¹⁹ The host-subtracted photometry from ZTF and the FORS2 photometry indicate $(g - r) \lesssim -0.5 \text{ mag}$ throughout the evolution following the light-curve peak. Such a blue color is not normally seen in regular SESNe at epochs postpeak. Indeed, even at 2–3 weeks before maximum light, such a blue color is rare, and the color index usually stays $>0 \text{ mag}$ throughout the SN evolution (e.g., Taddia et al. 2015; Zheng et al. 2022).

During the decay phase, the light curves show possible flattening leading to a tail phase slope shallower than the ^{56}Co decay rate assuming complete γ -ray trapping (Figure 2(b), inset). A decay rate slower than ^{56}Co decay indicates that the light curve is not powered solely by radioactive decay and thus

may also be powered by other processes, e.g., late-time ejecta–CSM interaction (e.g., Maeda et al. 2015; Dessart et al. 2022) or magnetar spin-down (e.g., Afsariardchi et al. 2021). The blue color is reminiscent of the interaction-powered Type Ib/Icn SNe (see, e.g., Ho et al. 2021, Figure 12), suggesting that a similar powering mechanism is likely to be at play.

3.2. Nebular Spectrum

The nebular spectrum of SN 2021ocs, obtained +148 days after the o -band peak, shows characteristics not regularly seen in an SESN nebular spectrum. While the latter is typically dominated by strong emission lines of the [O I] $\lambda\lambda 6300, 6364$ doublet, [Ca II] $\lambda\lambda 7292, 7324$ doublet, and Ca II $\lambda\lambda 8498, 8542, 8662$ triplet, SN 2021ocs shows a spectrum with more than five emission lines of similar strength across the spectrum (Figure 3). Such a spectrum has never been seen among ~ 200 SESN nebular spectra in the literature (Taubenberger et al. 2009; Fang et al. 2022; Prentice et al. 2022), suggesting a very rare occurrence rate of under 1%. It is also markedly different compared to the nebular spectra of Type Ia SNe, which are dominated by Fe-peak elements (e.g., Taubenberger et al. 2013). Strong H emission lines are absent in SN 2021ocs, which supports the initial SESN classification. The emission lines in the spectrum may be attributed to different transitions and ionization states of O, i.e., O I, [O I], [O II], and [O III], with similar line widths of $\sim 6000 \text{ km s}^{-1}$ (FWHM). The commonly seen [O I] $\lambda\lambda 6300, 6364$ doublet is present, possibly superposed on a broader base extending to $\pm 12,000 \text{ km s}^{-1}$ that may be attributed to Fe II (Dessart et al. 2021). The [O II] $\lambda\lambda 7320, 7330$ is present and likely to be blended with the commonly seen [Ca II] $\lambda\lambda 7292, 7324$. It is clear that the [O I] $\lambda\lambda 6300,$

¹⁸ Obtained from the Open Astronomy Catalog API, <https://github.com/astrocatalogs/OACAPI>.

¹⁹ Note that there is no r -band detection in the ZTF public data stream; see, e.g., <https://alerce.online/object/ZTF21abhprja>.

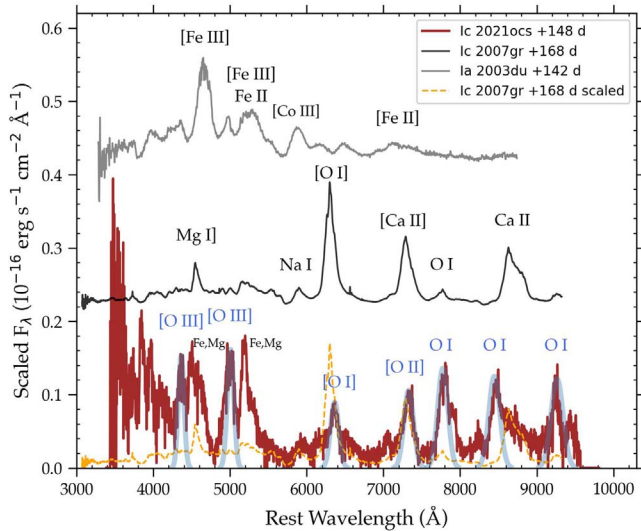


Figure 3. Nebular spectrum of SN 2021ocs (red) compared to typical nebular spectra of SNe Ic and Ia at similar epochs. The comparison spectra are of SNe 2007gr (black; Shivvers et al. 2019) and 2003du (gray; Stanishev et al. 2007), taken from WiSeREP. The spectrum of SN 2021ocs shows a number of O lines with superposed model lines, assuming a Gaussian profile with FWHM = 6000 km s⁻¹ (light blue). The flux of the spectrum of SN 2007gr is scaled to match the *r*-band magnitude of SN 2021ocs at +148 days; the spectrum is plotted twice for clarity of the comparison.

(The data used to create this figure are available.)

6364 and [Ca II] $\lambda\lambda 7292, 7324$ lines are not the strongest lines in the nebular spectrum, which is atypical for SESNe. Furthermore, the flux ratio of [O I] $\lambda\lambda 6300, 6364$ to [Ca II] $\lambda\lambda 7292, 7324$ is typically >1 for Type Ic SNe (e.g., Fang et al. 2022), which is not the case in SN 2021ocs.

In the red part of the spectrum, three permitted O I emission lines are seen at $\lambda\lambda 7774, 8446, \text{ and } 9263$.²⁰ While the O I $\lambda 7774$ is weak in SESNe nebular spectra, it is exceptionally strong in SN 2021ocs, suggesting high-density conditions. This line is possibly contaminated by Mg I $\lambda\lambda 7877, 7896$ in the red shoulder (Figure 4). The $\lambda 8446$ line is similarly contaminated by the broad Ca II triplet on the red side (see comparison with scaled SN 2007gr in Figure 3), although the peak is still clearly prominent. The [O I] $\lambda 9263$ line is blended with Mg II $\lambda 9224$. The peak intensities of the [O I] $\lambda 8446$ and $\lambda 9263$ lines are similar to the O I $\lambda 7774$ line. In typical SESNe, these two redder lines are either very weak or missing. These three O I lines are considered as the most persistent lines of oxygen in the optical and near-infrared regimes, as they appear over a broad range of conditions in spectroscopic experiments (Sansonetti & Martin 2005).

In the blue, two broad [O III] emission lines are seen, the $\lambda\lambda 4959, 5007$ doublet and $\lambda 4363$. They are accompanied by broader emission lines on the red side ($\sim 4600, 5200 \text{ \AA}$), possibly arising from the Fe I/Fe II complexes (see, e.g., Figure 7 of Dessart et al. 2021), with prominent peaks of Mg I and Mg II at $\lambda\lambda 4481, 4571, \text{ and } 5170$. Broad [O III] at late phase is also seen in a number of interacting SESNe, e.g., SN 1993J (Matheson et al. 2000) and SN 2014C (Milisavljevic et al. 2015). The Mg appears conspicuously in the spectrum of SN 2021ocs, with other lines at $\lambda\lambda 3832$ (triplet), 8224 (possible blend with [O I] $\lambda 8221$), and 9436 (doublet). The Mg emission lines are also seen weakly in some SNe Ibn such as SN 2006jc (Pastorello et al. 2007).

²⁰ These lines are themselves multiplets of several oxygen transitions.

3.3. Interpretation: CSM Interaction or a Pulsar Wind Nebula?

Comparing the nebular spectrum of SN 2021ocs to a number of interacting SNe yields few similarities while the spectrum remains unique and unparalleled in the literature. The blue color and light-curve flattening in SN 2021ocs may be explained by CSM interaction, which warrants a spectral comparison with interacting SNe. Figure 4 shows the SN 2021ocs spectrum compared to interacting SNe of Types IIn, Ibn, and Icn that have relatively good coverage in late phases.²¹

The strong narrow H emission lines defining the Type IIn SNe (Schlegel 1990) are clearly absent in SN 2021ocs. The SNe Ibn show prominent narrow He emission lines and a rising blue part of the spectrum (Pastorello et al. 2007), which originates from Fe emission (Dessart et al. 2021, 2022). Similarly, this blue rise is also seen in SN 2021ocs, while strong He lines are absent except for the weak He I $\lambda 7065$ and $\lambda 5876$, which is blended with the Na I doublet $\lambda\lambda 5890, 5896$. Also, He I $\lambda 5016$ may be contaminating the [O III] doublet $\lambda\lambda 4959, 5007$. The weak He lines in the spectrum of SN 2021ocs suggest that little He is present.

Similar to SNe IIn and Ibn, SNe Icn (Gal-Yam et al. 2022) also show the Fe bumps at late time. In SNe Icn, the initially strong lines of ionized C disappear at later phases to give way to nebular O I lines in the red part of the spectrum. These O I lines are present in SN 2021ocs, which may suggest a connection to SNe Icn, which are interpreted as explosions of W-R stars within a H/He-deficient CSM. Considering the spectra and light curves, it is possible that SN 2021ocs fits this scenario as well, although the CSM interaction did not occur immediately after the explosion. The expanding ejecta interacted with H/He-poor CSM, and the interaction drove a reverse shock that ionized the O/Mg-rich outer part of the ejecta. Clumping and inhomogeneity in the ejecta, CSM, and ⁵⁶Ni distribution would cause different levels of compression and ionization stages in the gas, which could give rise to the various ionization states seen in the O and Mg emission lines. The absence/weakness of C and He lines sets SN 2021ocs apart from the general population of SNe Ibn and Icn.

Broad [O III] $\lambda\lambda 4959, 5007$ emission is usually only seen in very late times in CCSNe, a few years after the explosion, and has been interpreted as evidence of a pulsar/magnetar wind nebula (Chevalier & Fransson 1992; Milisavljevic et al. 2018) alternative to CSM interaction. In this case, the line is also accompanied by [O I] and [O II], which is interpreted as different ionization layers by photoionization. The [O III] line is seen in a variety of SESNe, including the normal and superluminous ones (Milisavljevic et al. 2018). This subset of objects that show broad late-time [O III] curiously display a narrow ($\sim 2000 \text{ km s}^{-1}$) and relatively strong O I $\lambda 7774$ line in the nebular phase around a half to 1 yr postexplosion, although in these cases, it is neither strong nor accompanied by the same set of lines seen in SN 2021ocs. Figure 5 shows the nebular spectrum of SN 2021ocs compared to such objects. Generally, the agreement is poor; while they show similar line profiles in [O II] $\lambda\lambda 7320, 7330$ (sloping blue shoulder, contamination by [Ca II]) and O I $\lambda 7774$ (sloping red shoulder, contamination by Mg II), striking differences are seen in the O I $\lambda 8446$ line, Mg

²¹ Some objects (i.e., SNe 2006jc and 2019hgp in this case) evolve more rapidly; thus, the phases in days are shorter compared to the slower-evolving objects.

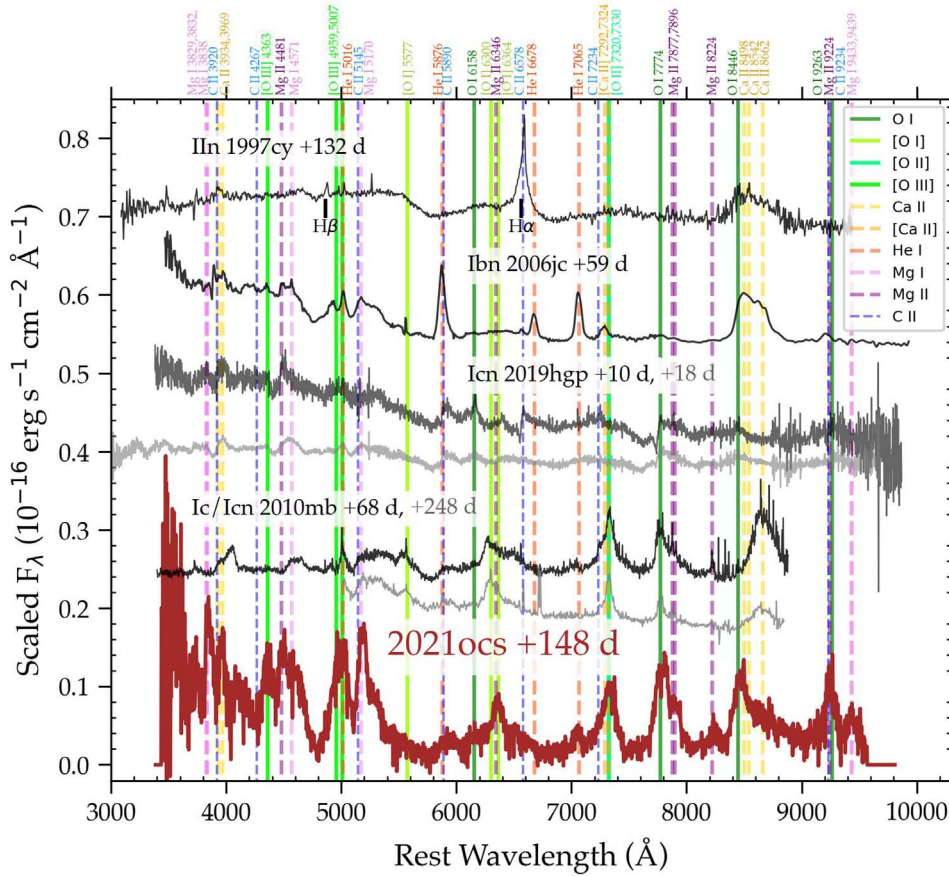


Figure 4. Comparison of the SN 2021ocs spectrum with interacting SNe of Types IIn (SN 1997cy; Turatto et al. 2000), Ibn (SN 2006jc; Pastorello et al. 2007), and Icn (SN 2019hgp, Gal-Yam et al. 2022; SN 2010mb, Ben-Ami et al. 2014). The epochs are relative to maximum light. Spectra were taken from WISeREP. Significant emission lines are identified.

lines redward of 8000 \AA , and the various strong lines in the blue, which all are absent or very weak in the comparison objects. The association of SN 2021ocs with a wind nebula caused by a magnetized central object is therefore weak, and CSM interaction remains as our preferred interpretation of the observed properties in the spectra and light curves. Drawing an analogy with Type Ibn/Icn SNe (e.g., Pastorello et al. 2007; Ben-Ami et al. 2014; Ho et al. 2021; Gal-Yam et al. 2022), SN 2021ocs shows a similarly blue ($g - r$) color, a rising blue continuum possibly extending to the ultraviolet (see interaction models of Dessart & Hillier 2022), and prominent emission lines of O and Mg, suggesting a similar mechanism of CSM interaction. Even with CSM interaction, SN 2021ocs appears to be underluminous ($M_o = -16.7$ mag, compared to $M_R = -17.9 \pm 0.7$ mag for SNe Ic in the sample of Zheng et al. 2022). This suggests a small amount of ^{56}Ni , which is another similarity to SNe Ibn and Icn.

In SN 2021ocs, the CSM interaction likely occurred past the light-curve peak. Clearly, if interaction is present, it cannot be strong early on. A delayed interaction may be interpreted as a detached or low-density nearby CSM, which was surrounding the SN progenitor star at the time of explosion. Furthermore, for the interaction to be dominating at late times, the amount of CSM must be small (see, e.g., Dessart et al. 2022). Assuming an ejecta velocity of $10,000 \text{ km s}^{-1}$, if CSM interaction started ~ 50 days after the explosion, as inferred from the blue ($g - r$) color, then the distance traversed by the unimpeded SN ejecta would be $\sim 4 \times 10^{15} \text{ cm}$ from the progenitor star. This inferred

CSM distance is similar to those in other interacting SESNe with detached CSM (e.g., SN 2017dio; Kuncarayakti et al. 2018). In the case of SN 2021ocs, as a Type Ic SN, its progenitor could have been a carbon–oxygen star with a wind velocity of $\sim 1000 \text{ km s}^{-1}$. If the CSM was formed through such a wind, the mass loss probed by the CSM interaction would have occurred ~ 500 days before the SN. At this time, the progenitor star would have just finished the C-shell burning stage and starting Ne burning (Fuller 2017). The short CSM distance and time before the SN explosion indicate that the SN progenitor star could have been surrounded by CSM at the time of explosion, although not as embedded as in the case of SNe Icn/Ibn, which show a rapidly increasing CSM density toward the SN progenitor (steeper than r^{-2} ; Maeda & Moriya 2022). The immediate circumstellar environment of SN 2021ocs, therefore, was relatively clean compared to those of SNe Icn/Ibn, as the explosion was first seen as a normal Type Ic SN without CSM interaction. This suggests that the CSM density was low closer to the progenitor star, implying a possible CSM distribution in a detached torus or disk, clumps, or a shell, which in any case contains a central cavity. Two possible interpretations arise regarding the progenitor mass loss as it approaches the terminal explosion: (1) a low progenitor mass-loss rate, suggesting that mass loss may have become weaker once the stripping reached the inner O–Mg core, or (2) the progenitor ejected some material that pushed away slower CSM in the vicinity, creating a cavity. In either case, SN 2021ocs represents the most extreme case of envelope

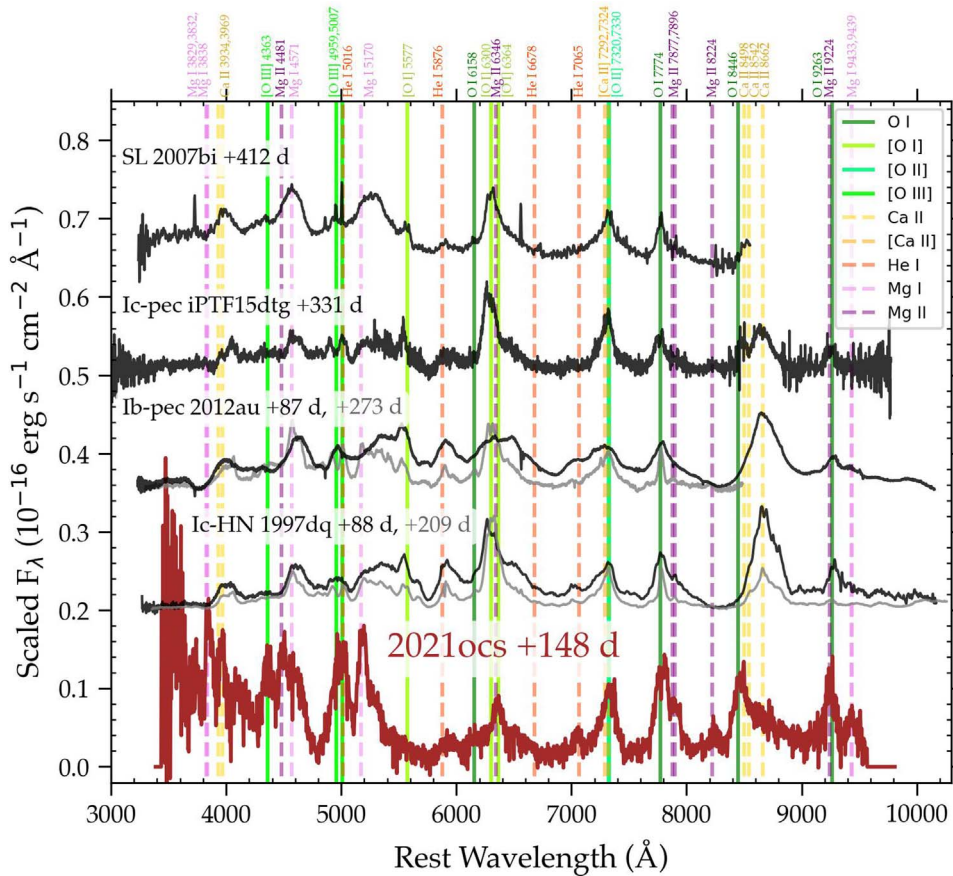


Figure 5. Comparison of the SN 2021ocs spectrum with SNe harboring a pulsar/magnetar wind nebula in the sample of Milisavljevic et al. (2018): SN 2007bi (SLSN-I; Gal-Yam et al. 2009), iPTF15dtg (Ic with broad light curves; Taddia et al. 2019), SN 2012au (Ib-peculiar; Milisavljevic et al. 2018), and SN 1997dq (Ic-hypernova; Matheson et al. 2001; Taubenberger et al. 2009). The epochs are relative to maximum light. Spectra were taken from WISEREP. Significant emission lines are identified.

stripping where the O–Mg layer of the progenitor is exposed. Within the massive star SN ejecta–CSM interaction case, it is positioned at the end of the sequence of CSM buildup resulting from the progenitor stripping: IIn \rightarrow Ibn \rightarrow Icn \rightarrow SN 2021ocs.

4. Summary

This letter presents photometry and spectroscopy of SN 2021ocs that yield a peculiar nebular spectrum dominated by O and Mg emission lines. The unique set of emission lines, blue continuum and color, and slowly declining light-curve tail suggest that interaction with a H/He-poor CSM took place in SN 2021ocs. The absence of signs of interaction in the early spectrum suggests that the CSM density close to the progenitor star was low. Comparing with interacting SESNe of Types Ibn and Icn, SN 2021ocs appears to be more stripped as the deep O–Mg layer in the progenitor is exposed, and the outer C–O and He-rich layers are stripped away. The SN 2021ocs poses yet another challenge to stellar evolution theory regarding the final phases of evolution of massive stars. With its unique spectral and photometric behavior, it represents a rare case not previously considered. Modeling the evolutionary pathways, mass loss, and explosion of a highly stripped star with an exposed O–Mg layer will provide insights in comparison with the observations. Future observations of transients should consider targets with unusual colors, albeit a spectroscopically normal appearance, in order to uncover similar peculiar objects.







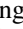




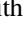

The anonymous referee is thanked for the useful feedback that substantially improved the paper. Stephen Smartt, Masaomi Tanaka, and Lucy McNeill are thanked for the discussions and suggestions on the paper. H.K. and T.N. were funded by the Academy of Finland projects 324504 and 328898. The work is supported by the JSPS Open Partnership Bilateral Joint Research Project between Japan and Finland (JPJSBP120229923). K.M. acknowledges support from the Japan Society for the Promotion of Science (JSPS) KAKENHI grants JP18H05223 and JP20H00174. S.M. acknowledges support from the Academy of Finland project 350458. R.K. acknowledges support from the Academy of Finland project 340613. This work has made use of data from the Asteroid Terrestrial-impact Last Alert System (ATLAS) project. The ATLAS project is primarily funded to search for near-Earth asteroids through NASA grants NN12AR55G, 80NSSC18K0284, and 80NSSC18K1575; by-products of the NEO search include images and catalogs from the survey area. This work was partially funded by Kepler/K2 grant J1944/80NSSC19K0112, HST GO-15889, and STFC grants ST/T000198/1 and ST/S006109/1. The ATLAS science products have been made possible through the contributions of the University of Hawaii Institute for Astronomy, the Queen’s University Belfast, the Space Telescope Science Institute, the South African Astronomical Observatory, and the Millennium Institute of Astrophysics (MAS), Chile. The Pan-STARRS1 Surveys (PS1) and the PS1 public science archive have been

made possible through contributions by the Institute for Astronomy, the University of Hawaii, the Pan-STARRS Project Office, the Max Planck Society and its participating institutes, the Max Planck Institute for Astronomy, Heidelberg and the Max Planck Institute for Extraterrestrial Physics, Garching, The Johns Hopkins University, Durham University, the University of Edinburgh, the Queen's University Belfast, the Harvard-Smithsonian Center for Astrophysics, the Las Cumbres Observatory Global Telescope Network Incorporated, the National Central University of Taiwan, the Space Telescope Science Institute, the National Aeronautics and Space Administration under grant No. NNX08AR22G issued through the Planetary Science Division of the NASA Science Mission Directorate, National Science Foundation grant No. AST-1238877, the University of Maryland, Eotvos Lorand University (ELTE), the Los Alamos National Laboratory, and the Gordon and Betty Moore Foundation. The ZTF forced photometry service was funded under Heising-Simons Foundation grant No. 12540303 (PI: Graham). This work was funded by ANID, Millennium Science Initiative, ICN12_009.

Facilities: VLT:Antu(FORS2), UH:2.2m(SNIFS), PS1.

Software: IRAF (Tody 1986, 1993), ESOReflex (Freudling et al. 2013).

ORCID iDs

H. Kuncarayakti  <https://orcid.org/0000-0002-1132-1366>
 K. Maeda  <https://orcid.org/0000-0003-2611-7269>
 L. Dessart  <https://orcid.org/0000-0003-0599-8407>
 T. Nagao  <https://orcid.org/0000-0002-3933-7861>
 M. Fulton  <https://orcid.org/0000-0003-1916-0664>
 M. E. Huber  <https://orcid.org/0000-0003-1059-9603>
 D. R. Young  <https://orcid.org/0000-0002-1229-2499>
 R. Kotak  <https://orcid.org/0000-0001-5455-3653>
 J. P. Anderson  <https://orcid.org/0000-0003-0227-3451>
 H. Gao  <https://orcid.org/0000-0003-1015-5367>
 E. Magnier  <https://orcid.org/0000-0002-7965-2815>
 K. W. Smith  <https://orcid.org/0000-0001-9535-3199>
 S. Srivastav  <https://orcid.org/0000-0003-4524-6883>

References

Afsariardchi, N., Drout, M. R., Khatami, D. K., et al. 2021, *ApJ*, **918**, 89
 Appenzeller, I., Fricke, K., Fürtig, W., et al. 1998, *Msngr*, **94**, 1
 Bellm, E. C., Kulkarni, S. R., Graham, M. J., et al. 2019, *PASP*, **131**, 018002
 Ben-Ami, S., Gal-Yam, A., Mazzali, P. A., et al. 2014, *ApJ*, **785**, 37
 Blondin, S., & Tonry, J. L. 2007, *ApJ*, **666**, 1024
 Chambers, K. C., Magnier, E. A., Metcalfe, N., et al. 2016, arXiv:1612.05560
 Chevalier, R. A., & Fransson, C. 1992, *ApJ*, **395**, 540
 Davis, K. W., Taggart, K., Tinyanont, S., et al. 2022, arXiv:2211.05134
 Dessart, L., & Hillier, D. J. 2022, *A&A*, **660**, L9

Dessart, L., Hillier, D. J., Sukhbold, T., Woosley, S. E., & Janka, H. T. 2021, *A&A*, **656**, A61
 Dessart, L., John Hillier, D., & Kuncarayakti, H. 2022, *A&A*, **658**, A130
 Fang, Q., Maeda, K., Kuncarayakti, H., et al. 2022, *ApJ*, **928**, 151
 Freudling, W., Romaniello, M., Bramich, D. M., et al. 2013, *A&A*, **559**, A96
 Fuller, J. 2017, *MNRAS*, **470**, 1642
 Gal-Yam, A., Bruch, R., Schulze, S., et al. 2022, *Natur*, **601**, 201
 Gal-Yam, A., Mazzali, P., Ofek, E. O., et al. 2009, *Natur*, **462**, 624
 Ho, A. Y. Q., Perley, D. A., Gal-Yam, A., et al. 2021, arXiv:2105.08811
 Hosseinzadeh, G., Arcavi, I., Valenti, S., et al. 2017, *ApJ*, **836**, 158
 Huber, M. E. 2021, *TNSCR*, **2021-2064**, 1
 Hunter, D. J., Valenti, S., Kotak, R., et al. 2009, *A&A*, **508**, 371
 Kool, E. C., Karamehmetoglu, E., Sollerman, J., et al. 2021, *A&A*, **652**, A136
 Kuncarayakti, H., Maeda, K., Ashall, C. J., et al. 2018, *ApJL*, **854**, L14
 Lantz, B., Aldering, G., Antilogus, P., et al. 2004, *Proc. SPIE*, **5249**, 146
 Maeda, K., Hattori, T., Milisavljevic, D., et al. 2015, *ApJ*, **807**, 35
 Maeda, K., & Moriya, T. J. 2022, *ApJ*, **927**, 25
 Masci, F. J., Laher, R. R., Rusholme, B., et al. 2019, *PASP*, **131**, 018003
 Matheson, T., Filippenko, A. V., Barth, A. J., et al. 2000, *AJ*, **120**, 1487
 Matheson, T., Filippenko, A. V., Li, W., Leonard, D. C., & Shields, J. C. 2001, *AJ*, **121**, 1648
 Milisavljevic, D., Margutti, R., Kamble, A., et al. 2015, *ApJ*, **815**, 120
 Milisavljevic, D., Patnaude, D. J., Chevalier, R. A., et al. 2018, *ApJL*, **864**, L36
 Modjaz, M., Blondin, S., Kirshner, R. P., et al. 2014, *AJ*, **147**, 99
 Pastorello, A., Smartt, S. J., Mattila, S., et al. 2007, *Natur*, **447**, 829
 Pellegrino, C., Howell, D. A., Terreran, G., et al. 2022, *ApJ*, **938**, 73
 Perley, D. A., Fremling, C., Sollerman, J., et al. 2020, *ApJ*, **904**, 35
 Perley, D. A., Sollerman, J., Schulze, S., et al. 2022, *ApJ*, **927**, 180
 Prentice, S. J., Maguire, K., Siebenaler, L., & Jerkstrand, A. 2022, *MNRAS*, **514**, 5686
 Sanders, N. E., Soderberg, A. M., Foley, R. J., et al. 2013, *ApJ*, **769**, 39
 Sansonetti, J. E., & Martin, W. C. 2005, *JPCRD*, **34**, 1559
 Schlafly, E. F., & Finkbeiner, D. P. 2011, *ApJ*, **737**, 103
 Schlegel, E. M. 1990, *MNRAS*, **244**, 269
 Shivvers, I., Filippenko, A. V., Silverman, J. M., et al. 2019, *MNRAS*, **482**, 1545
 Smith, K. W., Smartt, S. J., Young, D. R., et al. 2020, *PASP*, **132**, 085002
 Smith, N. 2014, *ARA&A*, **52**, 487
 Smith, N. 2017, in *Handbook of Supernovae*, ed. A. W. Alsabti & P. Murdin (Berlin: Springer), 403
 Smith, N., Li, W., Filippenko, A. V., & Chornock, R. 2011, *MNRAS*, **412**, 1522
 Stanishev, V., Goobar, A., Benetti, S., et al. 2007, *A&A*, **469**, 645
 Taddia, F., Sollerman, J., Fremling, C., et al. 2019, *A&A*, **621**, A64
 Taddia, F., Sollerman, J., Leloudas, G., et al. 2015, *A&A*, **574**, A60
 Taubenberger, S., Kromer, M., Pakmor, R., et al. 2013, *ApJL*, **775**, L43
 Taubenberger, S., Valenti, S., Benetti, S., et al. 2009, *MNRAS*, **397**, 677
 Theureau, G., Hanski, M. O., Coudreau, N., Hallet, N., & Martin, J. M. 2007, *A&A*, **465**, 71
 Tody, D. 1986, *Proc. SPIE*, **627**, 733
 Tody, D. 1993, in *ASP Conf. Ser. 52, Astronomical Data Analysis Software and Systems II*, ed. R. J. Hanisch, R. J. V. Brissenden, & J. Barnes (San Francisco, CA: ASP), 173
 Tonry, J. L., Denneau, L., Heinze, A. N., et al. 2018, *PASP*, **130**, 064505
 Tucker, M. A., Shappee, B. J., Huber, M. E., et al. 2022, arXiv:2210.09322
 Turatto, M., Suzuki, T., Mazzali, P. A., et al. 2000, *ApJ*, **534**, L57
 Woosley, S. E., Langer, N., & Weaver, T. A. 1995, *ApJ*, **448**, 315
 Yaron, O., & Gal-Yam, A. 2012, *PASP*, **124**, 668
 Yoon, S. C., Woosley, S. E., & Langer, N. 2010, *ApJ*, **725**, 940
 Zheng, W., Stahl, B. E., de Jaeger, T., et al. 2022, *MNRAS*, **512**, 3195